

Experimental and computational studies of the hydrogenation of carbon disulfide (CS₂) on ice analogues

Thanh Nguyen¹* †, Germán Molpeceres², Yasuhiro Oba¹, Marcelino Agúndez², Gisela Esplugues^{3,4}, José Cernicharo², and Naoki Watanabe¹

¹ Institute of Low Temperature Science, Hokkaido University, Kita 19, Nishi 8, 060-0819, Sapporo, Japan

² Instituto de Física Fundamental, CSIC, Calle Serrano 123, E-28006, Madrid, Spain

³ Observatorio Astronómico Nacional (OAN), Alfonso XII, 3, 28014 Madrid, Spain

⁴ Observatorio de Yebes, IGN, Cerro de la Palera s/n, E-19141 Yebes, Guadalajara, Spain

Accepted 2026 February 23. Received 2026 February 23; in original form 2025 December 21

ABSTRACT

Carbon disulfide (CS₂) is one of the sulfur-bearing species expected to be present in the interstellar medium (ISM). In this study, we investigated the surface reactions of solid CS₂ with hydrogen (H) atoms on amorphous solid water (ASW) using laboratory experiments supported by computational calculations. Our results show that CS₂ reacts with H atoms through quantum tunneling in the initial step, followed by successive H addition reactions, with or without activation barriers, on icy surfaces. These processes lead to the formation of several sulfur-bearing species, including hydrogen sulfide (H₂S), methyl mercaptan (CH₃SH), and small amounts of dithioformic acid (HC(S)SH) and methanedithiol (CH₂(SH)₂). The observed reactivity of CS₂ with H atoms provides a plausible explanation for the non-detection of CS₂ in interstellar ices. Furthermore, the efficient hydrogenation of the complex molecules derived from CS₂, namely HC(S)SH and CH₂(SH)₂, suggests that these species could be easily undergone with H atoms to produce other S-bearing species under ISM conditions.

Key words: astrochemistry – ISM: clouds – ISM: molecules – ISM: atoms – solid state: volatile

1 INTRODUCTION

In recent years, sulfur (S) chemistry on icy grains mantles in dense clouds, prestellar cores, cometary ices, and planets has attracted increasing attention not only from the astrochemical community but also from the fields of astrobiology and planetary science (Mifsud et al. 2021). To date, more than 30 S-bearing species have been identified in the interstellar medium (ISM), and most of which have been detected only in the gas phase. Recent observations from the QUIJOTE line survey have identified many S-bearing species in dense clouds, such as NCS, HCCS, H₂CCS, H₂CCCS, C₄S, C₅S, HC-SCN, HCSCCH, and NCCHCS (Cernicharo et al. 2021a,c; Cabezas et al. 2024), NC₃S, HC₃S, and HNCS (Cernicharo et al. 2024a,b), CH₃CHS and CH₂CHCHS (Agúndez et al. 2025; Cabezas et al. 2025). However, the total observed abundance of S-bearing species in dense clouds remains significantly lower than the expected cosmic abundance of sulfur (Wakelam et al. 2004; Anderson et al. 2013; Fuente et al. 2023). This mismatch is commonly referred to as the “sulfur depletion problem” (Ruffle et al. 1999; Vidal et al. 2017; Laas & Caselli 2019), in which the “missing sulfur” is thought to be trapped within interstellar grains. The mechanisms driving the chemical conversion of sulfur-bearing species on grain surfaces remain poorly understood, hindering the identification of the specific compounds likely to be present in interstellar ices. Laboratory ex-

periments and computations have investigated surface processes for S-bearing species in the ISM. Some of these studies include chemical pathways starting from hydrogen sulfide (H₂S) and methyl mercaptan (CH₃SH) (Lamberts & Kästner 2017; Oba et al. 2018; Lamberts 2018; Nguyen et al. 2023). These two species are considered to form on dust grains (Millar et al. 1986; Millar & Herbst 1990; Lamberts 2018), they have been detected only in the gas phase, suggesting that they are desorbed into the gas phase or transformation into other S-bearing species by (non-)energetic processes in interstellar dust grains, as indicated in previous studies (Ferrante et al. 2008; Garozzo, M. et al. 2010; Jiménez-Escobar et al. 2014; Oba et al. 2018; Nguyen et al. 2023). In addition to H₂S and CH₃SH, carbonyl sulfide (OCS) and sulfur dioxide (SO₂) have been identified as dominant sulfur-bearing species in the solid phase. Several laboratory studies have demonstrated their formation via ion irradiation of S-containing species mixed with ice components or through S-ion implantation into O-bearing species (e.g., O₂, CO, and CO₂) (Ferrante et al. 2008; Mifsud et al. 2024). However, their abundances are estimated to be significantly lower than the total expected sulfur abundance, implying that the missing sulfur problem is present in icy grain mantles. A suggestion is that a substantial fraction of sulfur may be locked in refractory reservoirs or converted into other S-bearing species through (non-)energetic processing (Shingledecker et al. 2020; Mifsud et al. 2021; Mifsud et al. 2022). Indeed, surface reactions of OCS and SO₂ with H atoms have been investigated under conditions in the ISM, suggesting the formation of some S-bearing species such as HCSOH, HSOOH, and HOSOH, which, however, have not been detected yet in

* E-mail: tnguyen@strw.leidenuniv.nl

† Current address: Laboratory for Astrophysics, Leiden Observatory, Leiden University, PO. Box 9513, NL 2300 RA Leiden, The Netherlands.

the ISM (Molpeceres et al. 2021b, 2022; Nguyen et al. 2021, 2024). Some characteristic features of S-bearing molecules were found in previous laboratory studies (Nguyen et al. 2021, 2023, 2024), where S-bearing species including OCS, SO₂, and CH₃SH yielded H₂S as a final product after reacting with H atoms on interstellar ice analogs at low temperatures. After formation, H₂S can be easily desorbed into the gas phase by chemical desorption with the efficiency of $3 \pm 1.5\%$ per reaction (Oba et al. 2018; Furuya et al. 2022). Additionally, the absorption coefficient of H₂S has been investigated to be low in dense clouds and solid H₂S can further react with other species on dust grains (e.g., NH₃) to form more complex molecules (e.g., ammonium salts, NH₄SH; Slavicinska et al. (2025)). Alternatively, H₂S can be converted to the high-molecular-weight S-containing molecules, including sulfanes (H₂S_n; n = 2-11) and octasulfur (S₈), by galactic cosmic ray processing on icy dust grains (Herath et al. 2025). These processes can collectively contribute to explaining the "sulfur depletion problem" in dense clouds. The preferential formation of H₂S, a simpler molecule than its precursors (e.g., OCS, CH₃SH, SO₂; Nguyen et al. 2021, 2023, 2024), together with its potential for chemical desorption, is intriguing and may partly account for the missing sulfur in dark clouds.

In this context, carbon disulfide (CS₂) emerges as a promising candidate for advancing our understanding of the resilience of sulfur-bearing molecules on interstellar ices. The existence of CS₂ in cometary ices has been proposed based on the detection of a high abundance of the CS molecule in comets, which is related with CS₂ (Despois et al. 1992; Feldman et al. 1980; Smith et al. 1980; Weaver et al. 1981). For instance, the abundance of CS₂ has been estimated to be approximately 0.2% relative to H₂O in comet C/1995 O1 (Hale-Bopp) (Bockelée-Morvan et al. 2000). With the *James Webb Space Telescope* (JWST), CS₂ has been detected in the atmosphere of the warm sub-Neptune TOI-270 d, in conjunction with other sulfur-bearing species, including CS and H₂CS (Moses et al. 2024; Felix et al. 2025). The detection of CS₂ on grains in low-temperature regions may provide valuable insights into S chemistry and could also be significant in less evolved regions, such as dark clouds. However, to date, neither CS₂, which lacks a permanent dipole moment, nor its protonated form, HSCS⁺, have been identified in the interstellar medium (ISM). Alternately, although the formation of CS₂ is proposed less effective in dense quiescent cloud, several previous studies have suggested that the lack of observational detection of CS₂ may result from the overlap of its infrared absorption bands with those of other species and/or its rapid conversion into other products shortly after formation (Garozzo, M. et al. 2010). Therefore, laboratory investigations of the chemical reactivity of CS₂ on interstellar dust grains are essential for understanding its astrochemical role.

Laboratory experiments indicated that CS₂ can be formed by ion irradiation of mixed ices containing H₂S with CO or by He⁺ ion irradiation of ice components (e.g., CO, CO₂) deposited on top layers of allotropic sulfur (Garozzo, M. et al. 2010; Mifsud et al. 2025). Additionally, CS₂ formation has been reported following proton irradiation of OCS (Ferrante et al. 2008), as shown in the reactions below occurring on ices:



Also, astrochemical models postulate that the main contributing grain

phase formation routes are (Laas & Caselli 2019):



Among these reactions, it is worth noting that those involving atomic carbon are likely less efficient, since atomic carbon is predominantly chemisorbed on dust grains (occupying more than 70% of binding sites according to Molpeceres et al. 2021a; Tsuge et al. 2023). However, in contrast to its formation processes, the reactions of CS₂ with other species have not been examined in detail, with, to the best of our knowledge, only a few studies addressing this topic through electron bombardment and thermal reaction experiments (Bohn et al. 1992; Tsuge & Lee 2017; Ward et al. 2012). More recently, the chemical behavior of CS₂ under energetic irradiation has been explored in laboratory experiments (Martín-Doménech et al. 2024; Basalgète et al. 2026).

In this study, we focus on the chemical reactions of solid CS₂ with H atoms on an icy surface at low temperatures (typically 10 K) using experimental methods supported by preliminary theoretical calculations to understand the physicochemical behavior of CS₂ in interstellar ice.

2 EXPERIMENTAL PROCEDURE

All experiments were performed using the Apparatus for Surface Reaction in Astrophysics (ASURA). The ASURA system described in detail (Watanabe et al. 2006; Nagaoka et al. 2007; Nguyen et al. 2020, 2021, 2023, 2024). In brief, it is composed of an ultrahigh vacuum chamber with a base pressure of 1×10^{-8} Pa, an aluminum (Al) substrate mounted on a He cryostat, an atomic source, a Fourier-transform infrared spectrometer (FTIR), and a quadrupole mass spectrometer (QMS). The surface temperature can be controlled from 5 to 300 K.

The chemical reactions of CS₂ with hydrogen atoms were investigated on a compact amorphous solid water (c-ASW) substrate at low temperatures (typically 10 K). The c-ASW was prepared by depositing H₂O vapor onto the surface at 110 K. The thickness of the c-ASW layer was estimated to be 20 monolayers (ML; 1 ML = 1×10^{15} molecules cm⁻²). After that, the surface temperature was lowered to 10 K for the investigation of the hydrogenation of CS₂. The number of monolayers corresponding to the H₂O ice thickness is estimated using the following equation (7):

$$N = 2.3 \times \frac{\sin(\theta) \times \int \text{Abs}(\nu) d\nu}{R \times A} \quad (7)$$

where $\int \text{Abs}(\nu) d\nu$ is the integrated absorbance of O-H stretching band at 3300 cm⁻¹, and A is the apparent band strength for transmission infrared spectroscopy (in molecule⁻¹cm), taken from the literature ($A = 2 \times 10^{-16}$ molecule⁻¹cm, Gerakines et al. 1995). For our FTIR setup, the correction factor, R, accounting for the conversion from transmission to reflection spectroscopy, was estimated to be 2.

Gaseous CS₂ was pre-deposited onto the c-ASW substrate at 10 K with a deposition rate of 1 ML minute⁻¹, resulting in an abundance of approximately 1 ML of CS₂. This was determined using the absorbance area of the C-S stretching band at 1540 cm⁻¹ and a band strength of 9.13×10^{-17} molecule⁻¹ cm (Garozzo et al. 2008). The pre-deposited CS₂ was exposed to hydrogen (H) or deuterium (D)

Table 1. Reaction energies (ΔU_R) and activation energies (ΔU_A) of the simplified reaction network presented in Figure 1. All energies are presented in kJ mol⁻¹. BL means barrierless. In barrierless reactions, the reaction energy is calculated from the energies of the separated reactants as $\Delta U_R = U_{AB} - (U_A + U_B)$ and in reactions with a barrier $\Delta U_R = U_{AB} - (U_{\text{PRC}})$ and $\Delta U_A = U - (U_{\text{PRC}})$, with PRC meaning pre-reactant complex and TS transition state.

Reaction	ΔU_R	ΔU_A
<i>First hydrogenation</i>		
CS ₂ + H \longrightarrow c-HSCS	-68.5	13.1
<i>Second hydrogenation</i>		
c-HSCS + H \longrightarrow t-HC(S)SH	-364.1	BL
c-HSCS + H \longrightarrow CS ₂ + H ₂	-357.8	BL
c-HSCS + H \longrightarrow H ₂ S + CS	-222.4	23.4
<i>Third hydrogenation</i>		
t-HC(S)SH + H \longrightarrow HSCHSH	-156.4	3.9
t-HC(S)SH + H \longrightarrow HSCH ₂ S	-164.0	22.3
t-HC(S)SH + H \longrightarrow c-HSCS + H ₂	-61.2	25.6
<i>Fourth hydrogenation</i>		
HSCHSH + H \longrightarrow CH ₂ (SH) ₂	-366.6	BL
SCH ₂ SH + H \longrightarrow CH ₂ (SH) ₂	-353.6	BL
SCH ₂ SH + H \longrightarrow t-HC(S)SH + H ₂	-258.1	12.1
SCH ₂ SH + H \longrightarrow H ₂ S + H ₂ CS	-280.3	1.1
<i>Fifth hydrogenation</i>		
CH ₂ (SH) ₂ + H \longrightarrow HSCHSH + H ₂	-57.7	29.2
CH ₂ (SH) ₂ + H \longrightarrow SCH ₂ SH + H ₂	-64.6	11.4

atoms for up to 2 hours to investigate the reaction kinetics. In a separate experiment, the gaseous CS₂ was co-deposited with H atoms on the c-ASW substrate at 10 K to increase the yields for better identifying the potential products from the chemical reactions of CS₂ with H atoms, and the deposition rates of CS₂ were approximately 0.08 or 1 ML min⁻¹ during the co-deposition.

H (or D) atoms were generated by dissociating H₂ (D₂) in a microwave-discharged plasma in the atomic source. The H (D) atoms were then cooled to 100 K through multiple collisions with the inner wall of an Al pipe connected to the atomic source, which was maintained at 100 K (Nagaoka et al. 2007). The fluxes of H and D atoms were estimated to be 1.4×10^{14} and 2.3×10^{14} cm⁻² s⁻¹, respectively, using the method outlined by Oba et al. (2014).

The chemical reactions of CS₂ with H (D) atoms were monitored in situ using FTIR with a resolution of 2 cm⁻². The reactants and products desorbed from the substrate were detected with the QMS through temperature programmed desorption (TPD) method at the ramping rate 4 K minutes⁻¹.

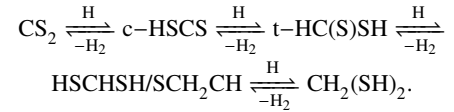
3 RESULTS AND DISCUSSIONS

3.1 Preliminary computational exploration of the CS₂ hydrogenation mechanism

Before examining the experimental evidence for CS₂ hydrogenation, we first performed a preliminary assessment of the most likely reaction pathways for this system. To this end, we carried out quantum chemical calculations using automated reaction discovery and simplified gas-phase models. The gas-phase approach serves as a first-order approximation to reactions occurring on ice surfaces, where reaction barriers can be modulated, as demonstrated in Molpeceres

et al. (2024). In that work, we showed that for a reaction network comprising 39 reactions, the deviation in activation barriers introduced by representing surface processes with a gas-phase model was, in the vast majority of cases, below 2 kcal mol⁻¹. This small discrepancy arises because, in such reactions, the ice matrix primarily acts as a molecular scaffold rather than as a true catalyst. Although the gas-phase model remains an approximation, its use is justified here by our goal of interpreting the experiments and by the inherent complexity of the reaction network. A more quantitative treatment is left for future dedicated work. We specifically employ the multi-component artificial induced reaction method (MC-AFIR) using the GRRM23 (Maeda et al. 2013, 2023b,a) coupled with the ORCA6.0.0 code (Neese 2022) using the ω B97M-V functional (Mardirossian & Head-Gordon 2016) using the def2-TZVPD basis set (Rappoport & Furche 2010). All calculations employ a γ collision parameter (see Maeda et al. 2013) of 250 kJ mol⁻¹ that roughly corresponds to the maximum energy barrier that could be overcome in the calculation. We studied the possible formation pathways sequentially, that is, we first investigated the products of the CS₂ + H reaction and later the hydrogenation of the products, up to the hydrogenation of CH₂(SH)₂. After the MC-AFIR calculations, the approximated transition states are refined at the same level of theory, following by an intrinsic reaction coordinate (IRC) and optimization of their endpoints to collect the reactants and product states of each reaction to determine the reaction and activation energies ΔU_R and ΔU_A .

The reaction network is extremely complex, spanning several tens of stationary points, including isomers, carbenes, conformers or hypervalent compounds. Therefore, for the sake of simplicity, in this work we summarize the results to the direct reaction pathway:



We will also highlight specific deviations from this scheme, such as the formation of H₂S + CS or H₂CS + H₂S, when relevant. A visual representation of the reaction network used to interpret our experimental results is provided in Figure 1 and Table 1. This reaction network successfully reproduces the experimental findings. In the first place, the reaction CS₂ + H \longrightarrow c-HSCS, overcoming a small barrier of 13.1 kJ mol⁻¹, presumably by the action of quantum tunneling as evinced by the experiments using deuterium shown in Section (3.2.3). Interestingly, as we observed in Molpeceres et al. (2021c) in the case of the hydrogenation of OCS, the addition product of the reaction yields exclusively the *cis* conformer of the HSCS radical. The formation of S(CH)S, CS₂ + H \longrightarrow S(CH)S, is much less effective than that of HSCS, owing to the high barrier (~ 41.8 kJ.mol⁻¹).

The c-HSCS radical can evolve in three different ways, first it can proceed without a barrier to CS₂ (H-abstraction) or to t-HC(S)SH (H-addition). Additionally, there is a channel with a moderate barrier to H₂S + CS, that is, an irreversible bimolecular channel. As we will show later, since there are available other low barrier fragmentation reactions we consider that the c-HSCS + H \longrightarrow H₂S + CS is not favored against the H-abstraction and H-addition reactions. Like in our previous investigations (Molpeceres et al. 2021c, 2025) we confirm that the H-addition of c-HSCS produce exclusively t-HC(S)SH that can continue reaction to two different radicals HSCHSH and SCH₂SH. While both channels have barriers, the H-addition to the sulfur atom (HSCHSH) is favored over the H-addition to the carbon atom (SCH₂SH), $\Delta U_A = 3.9$ kJ mol⁻¹ against $\Delta U_A = 22.3$ kJ mol⁻¹. It is important to note that 22.3 kJ mol⁻¹ is not extremely high and, as

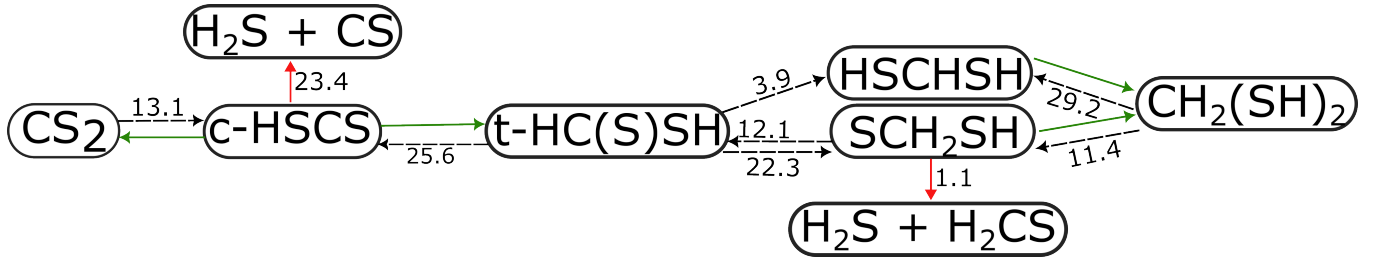
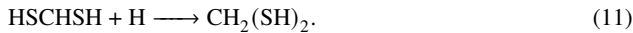


Figure 1. Summary of the simplified reaction network obtained in this work. Red arrows indicate irreversible pathways, green arrows indicate barrierless pathways and black dashed lines indicate reactions with a barrier, with the number representing the theoretically derived activation energy. Reactions from right to left occur with release of H_2 (hydrogen abstractions). Energies are shown in kJ mol^{-1} .

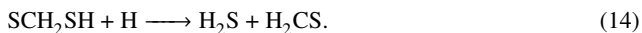
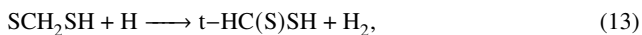
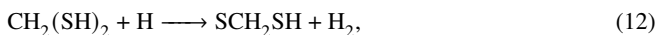
we explain in Molpeceres et al. (2025), the diffusion-reaction competition needs to be taken into account to discard possible reaction pathways. However, even if SCH_2SH is formed in appreciable amounts by this pathway, most of its abundance will come from a posterior reaction (see below). Additionally, we found a significant barrier for the H-abstraction reaction $\text{t-HC(S)SH} + \text{H} \rightarrow \text{c-HSCS} + \text{H}_2$ $\Delta U_A = 25.6 \text{ kJ mol}^{-1}$.

Considering the evolution from HSCHSH our MC-AFIR and subsequent geometry optimizations could only find the formation of methanedithiol ($\text{CH}_2(\text{SH})_2$), proceeding without a barrier. Thus, we can define a *forward* reaction network as:



that proceeds with low or no barriers. We note that some of these reactions are reiterative to the ones that will be presented in the experimental results section, but here are reproduced accounting for isomerism.

After formation, H-abstraction of $\text{CH}_2(\text{SH})_2$ may proceed via two possible pathways on the substrate. First, H-abstraction can take place at the $-\text{CH}_2-$ moiety and at the $-\text{SH}$ one. The H-abstraction at the SH moiety is clearly favored with a barrier of 11.4 kJ mol^{-1} against the 29.2 kJ mol^{-1} needed to abstract in the $-\text{CH}_2-$ group. Therefore, in contrast to what happens in the *forward* reaction network, the *reverse* reaction network initiated by $\text{CH}_2(\text{SH})_2$ favors the formation of SCH_2SH . This radical, contrary to the case of HSCHSH can experience H-abstraction reaction back to t-HC(S)SH , whose main hydrogenation pathways were explained above. More importantly, however, is the fact that SCH_2SH easily ($\Delta U_A = 1.1 \text{ kJ mol}^{-1}$) breaks irreversibly to form $\text{H}_2\text{S} + \text{H}_2\text{CS}$. Later H_2CS , through sequential hydrogenation, can easily form CH_3SH (Lamberts 2018). Therefore, the *reverse* reaction network would predominantly be described by:



The quantum chemical calculations presented here, despite simplified in relation to the total reaction network or choice of structural model, are able to explain the formation of all the closed shell molecules found in the experiment, H_2S , H_2CS , CH_3SH , HC(S)SH , and CHS(SH)_2 as we exemplify in the rest of the work.

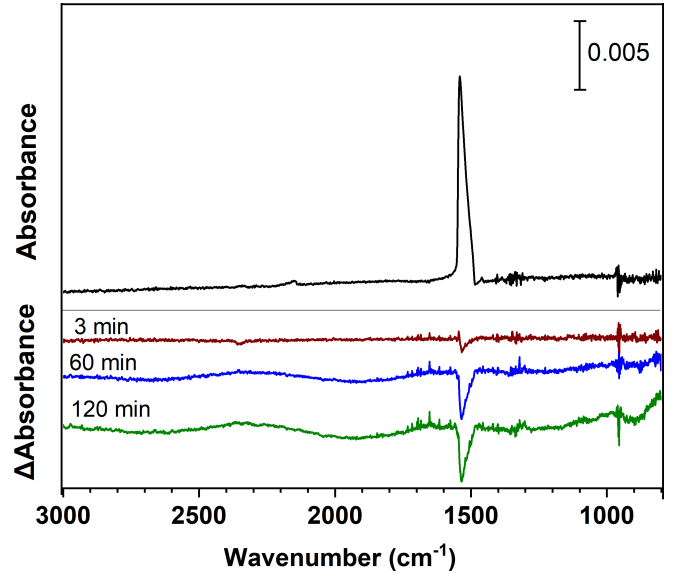


Figure 2. Variation in the different spectra of the solid CS_2 after exposure to H atoms for 3, 60, and 120 min at 10 K. A tiny absorption peak observed at 1304 cm^{-1} is assigned to CH_4 , which may be one of the products formed from reactions of CS_2 with H atoms.

3.2 Experimental results

3.2.1 Reactions of pre-deposition of CS_2 with H atoms on c-ASW at low temperatures

Figure 2 shows the variation in the FTIR spectra of solid CS_2 after exposure to H atoms for up to 2 hours, compared to the initial spectrum of unexposed CS_2 . The observed absorption peak at 1304 cm^{-1} (above the baseline) was attributed to the C-S stretching band of CS_2 , which aligned well with previous studies (Garozzo et al. 2008; Edridge 2010). The decrease in CS_2 intensity with exposure to H atoms indicated the loss of CS_2 due to reactions with H atoms on the substrate. In contrast, no distinct infrared features of S-containing products were observed, most likely due to the limited number densities of the products.

As discussed in Section 3.1, computational results indicate that reaction (8), in which an H atom adds to the S atom of CS_2 , has an activation barrier of 13.1 kJ mol^{-1} ($\sim 1575 \text{ K}$). In contrast, the activation barrier for reaction corresponding to H addition at the C atom, is considerably higher, about 41.8 kJ mol^{-1} ($\sim 5027 \text{ K}$). This difference suggests that solid CS_2 reacts preferentially with H

atoms at the sulfur site, forming the c-HSCS radical. We assume that reaction (8) proceeds at low temperatures with the aid of quantum tunneling, an assumption later confirmed in Section 3.2.3. Once formed, c-HSCS radicals can undergo further hydrogenation to yield new products. In comparison, the destruction to H₂S + CS involves moderate activation barriers (Figure 1). Moreover, the hydrogen abstraction merely returns to the starting point in the network (CS₂). These channels should therefore be less favorable than H addition. Consequently, HC(S)SH, produced via reaction (9), is expected to be the predominant product in the continuous hydrogenation of c-HSCS radicals.

Dithioformic acid (HC(S)SH) formed in reaction (9) is expected to further react with H atoms up to the formation of CH₂(SH)₂, which easily fragments to H₂S + H₂CS, and breaking the original CS₂ skeleton. The hydrogenation of H₂CS on the surface leads to the formation of CH₃SH, consistent with the quantum chemical results reported by Lamberts (2018), as follows:



On the other hand, H₂S is expected to desorb in the gas phase through chemical desorption (Oba et al. 2018):



where (g) is used to identify the release to the gas phase.

To verify the presence of these products after the pre-deposition experiments, we monitored the TPD-QMS profiles showing desorption peaks at $m/z = 16$ (CH₄), 34 (H₂S), and 48 (CH₃SH). The inclusion of CH₄ follows previous results (Nguyen et al. 2023), where it was identified as a fragmentation product of CH₃SH, as discussed in more detail below. All expected peaks were detected (Figure 3). In particular, the desorption peak at $m/z = 48$, observed between 90 and 115 K, corresponds to CH₃SH desorption (Figure 3a), in agreement with our earlier findings (Nguyen et al. 2023).

After formation on the icy substrate via H-abstraction reaction of SCH₂SH, H₂S can subsequently react with H atoms, leading to the loss of H₂S from the ice surface via chemical desorption (Oba et al. 2018, 2019). Figure 3b shows the desorption peak at $m/z = 34$ observed in the temperature in range of 80 - 95 K, which is attributed to H₂S remaining on the surface. The second peak, observed at approximately 95 - 130 K, corresponds to the fragment (³⁴S) from C³²S³⁴S. In addition, a small desorption peak (dashed black line in the H₂ case) at $m/z = 34$ in the temperature range of 75 - 85 K may indicate the contamination from the beam line. The production of H₂S from the reaction of CS₂ with H atoms is confirmed by the desorption peak at $m/z = 34$ in the TPD experiments. Figure 3c displays the desorption peak observed at $m/z = 16$ in the temperature range of 30 - 50 K, corresponding to the typical desorption temperature of CH₄, which is likely to proceed through the reaction of H atoms with CH₃ radical. These CH₃ radicals are yielded through CH₃SH with H atoms with low activation barriers or barrierless on c-ASW at 10 K following the reactions pathways by CH₃SH + H → CH₃ + H₂S and CH₃ + H → CH₄ (Qasim et al. 2020; Nguyen et al. 2023). Additionally, the H atoms landed on dust grains can efficiently consume trapped radicals and unsaturated species through addition and abstraction reactions, leading to smaller, stabilized products rather than larger species (Öberg et al. 2009), as supported by our computational results. In contrast, CS₂ polymerization typically requires energetic processing, such as UV irradiation or high-energy electrons (Cataldo 1995; Heymann et al. 2000). Therefore, CS₂ polymers cannot form under our present experimental conditions.

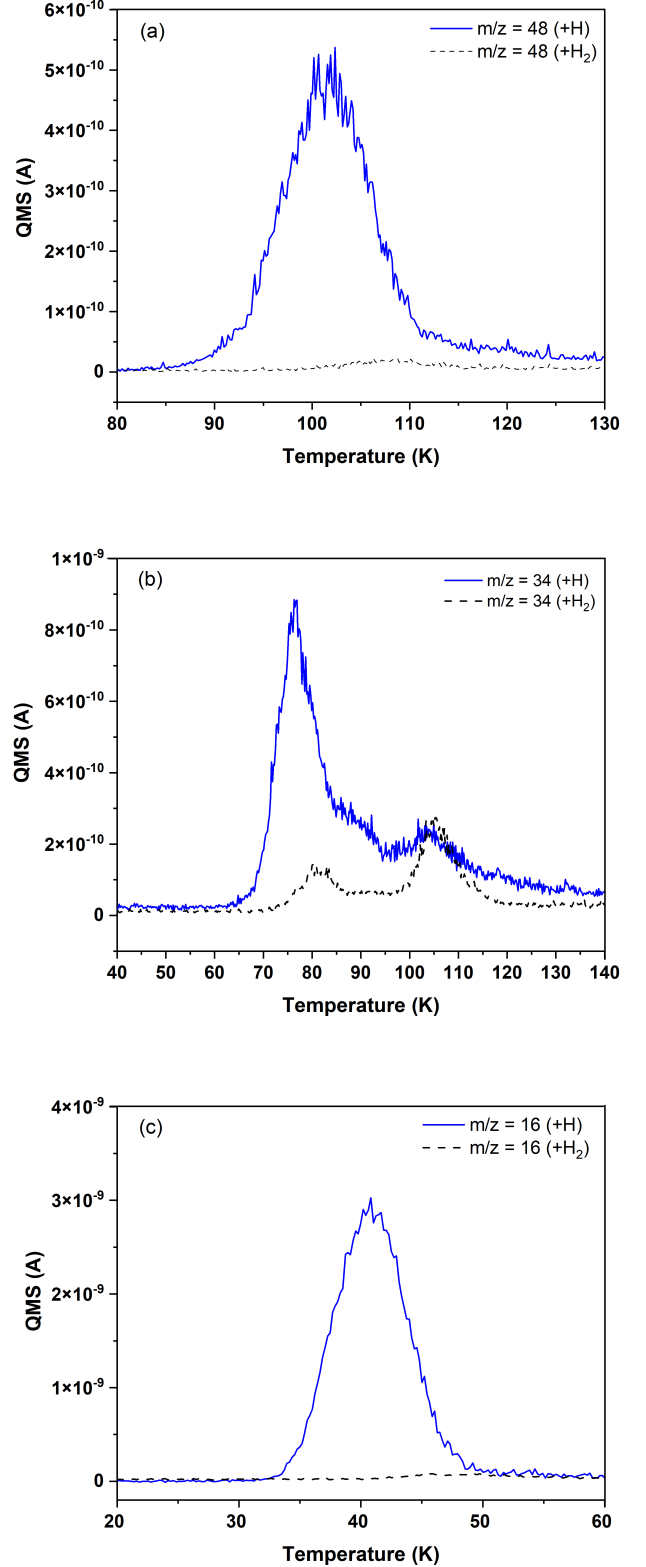


Figure 3. TPD-QMS spectra of the pre-deposited CS₂ with H atoms (solid blue lines), compared with H₂ molecules (dashed black lines), on c-ASW at 10 K for up to 2 h: (a) at $m/z = 48$ (for CH₃SH), (b) at $m/z = 34$ (for H₂S), and (c) at $m/z = 16$ (for CH₄).

The absence of observed IR features corresponding to HC(S)SH, CH₃SH, and H₂S from the reaction of pre-deposited CS₂ with H atoms is likely due to collisions and subsequent reactions of the products with other species (e.g., H atoms) on the substrate. These interactions may result in either insufficient accumulation of new species or chemical desorption of products into the gas phase, making them undetectable by FTIR. Additionally, the small amount of pre-deposited CS₂ (~1 ML) and the backward reaction that reforms CS₂ during the second hydrogenation step may further contribute to the lack of IR-detectable products. In order to shed further light into the products of the title reaction we perform additional experiments using co-deposition, indicated in Section 3.2.2.

3.2.2 Identification of products through co-deposition of CS₂ with H atoms on c-ASW at 10 K

In Figure (4), we show the FTIR spectrum of solid CS₂ (blue line) after co-deposition with H atoms for 2-hours on c-ASW at 10 K, and that with H₂ as a blank (back line) for comparison. The deposition rate of CS₂ was 0.08 ML min⁻¹. The co-deposition of CS₂ with H atoms resulted in the appearance of several new peaks, which were not observed in the blank.

Notably, several new bands appeared in the regions of approximately 3000–2800 cm⁻¹ and 1500–900 cm⁻¹ regions (see dashed arrows in Figure 4). These were reasonably assigned to methyl mercaptain (CH₃SH), based on the following vibrational bands: CH₃ anti-symmetric stretch (2997 cm⁻¹), CH₃ symmetric stretch (2929 cm⁻¹), CH₃ antisymmetric deformation (1432 cm⁻¹), CH₃ symmetric deformation (1320 cm⁻¹), and CH₃ rocking modes (1064–965 cm⁻¹) (Hudson 2016; Nguyen et al. 2023).

Although CH₃SH was not included in the possible reaction pathways shown in the previous section, it is likely that methanedithiol (CH₂(SH)₂) may react with H atoms to yield SCH₂SH radicals ($E_a = 11.4 \text{ kJ mol}^{-1}$), which would further react with H atoms with a negligible barrier (1.1 kJ mol⁻¹), resulting in the formation of H₂S and H₂CS (reaction 14). The hydrogenation of H₂CS, formed by reaction (14) can yield CH₃SH through reaction (15), as proposed by Lamberts (2018).

An absorption peak at 2540 cm⁻¹ observed after the co-deposition was attributed to the S–H stretching band in the products, such as H₂S and CH₃SH (Fathe et al. 2006; Oba et al. 2019; Nguyen et al. 2023). Furthermore, weak features at 2969 and 2838 cm⁻¹ were assigned to the CH₂ symmetric stretching band of H₂CS, which has been previously observed in the solid phase (Torres et al. 1982; Watanabe et al. 1991; Suzuki et al. 2007). The observed shifts in H₂CS absorption bands relative to the reference values were probably due to substrate-dependent effects during formation. In addition, a small peak observed at 1304 cm⁻¹ was assigned to CH₄ (Qasim et al. 2020).

Figure 5 displays the variation in the different spectra of the co-deposited CS₂ with H atoms at 10 K, recorded when the surface temperature was gradually warmed up from 10 to 170 K. The S–H stretching band at 2540 cm⁻¹ primarily decreases at temperatures below 110 K, suggesting the desorption of H₂S as reported by Oba et al. (2019). The desorption of CH₃SH completed in the temperature range of 110 – 125 K (Nguyen et al. 2023), which contributed to the decreases of the peak intensities at 2540, 3000 – 2800, and 1500 – 900 cm⁻¹ regions. These desorption temperatures align with the TPD signals observed at $m/z = 34$ and 48 (see Figure 3).

Figure 6a shows the FTIR spectrum of CS₂ co-deposited with H atoms at a high deposition rate, of CS₂ ~1ML min⁻¹, which is ~13 times higher than the previous experiments. By changing the deposi-

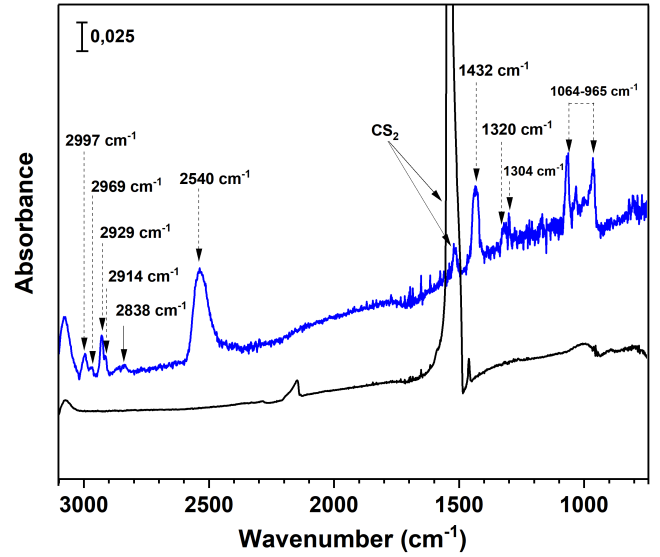


Figure 4. FTIR spectrum of the co-deposited CS₂ with H atoms (blue line) after 2 hours with a low deposition rate of 0.08 ML.min⁻¹ compared to the co-deposited CS₂ with H₂ (black line) on c-ASW at 10 K. The dashed arrows present the new features formed on the ice surface, they could be derived from the S-bearing species such as H₂S, CH₃SH, H₂CS, and CH₄. The solid arrows presents remaining CS₂ after 2 hours of the co-deposition.

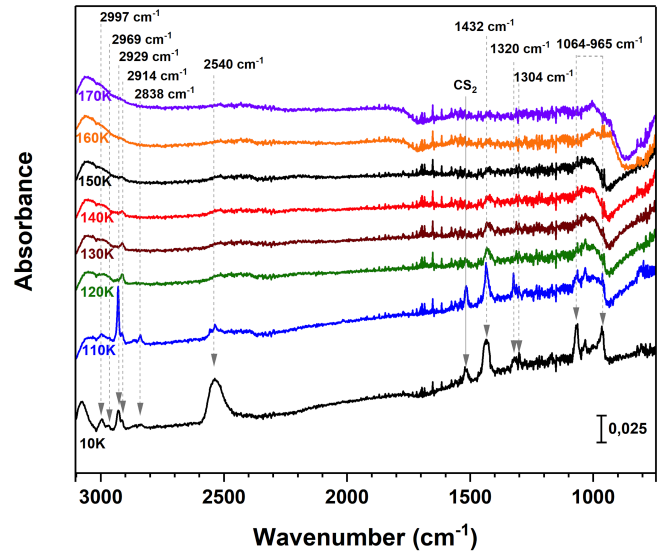
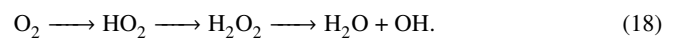


Figure 5. Variation of the different spectra of the sample for co-deposited CS₂ with H atoms at 10 K, recorded when the surface temperature was gradually warm up from 10 to 170 K.

tion rate of CS₂ (that of H was fixed at the constant rate), the absolute and relative yields of products can vary depending on the relative flux of the co-deposited species. For example, when oxygen molecules (O₂) and H atoms were co-deposited onto a reaction substrate at 10 K, hydrogen peroxide (H₂O₂) and water (H₂O) were formed as products through the following pathways:



where an arrow indicates an addition of one H atom to the reactant.

We have experimentally confirmed that the H₂O/H₂O₂ ratio in the products decreased with increasing the co-deposited O₂/H ratio (Oba et al. 2009). This is interpreted as follows: with increasing the O₂/H ratio, the number of H atoms which can react with formed H₂O₂ should decrease, resulting in the formation of less H₂O, that is, a low H₂O/H₂O₂ ratio in the product. Hence, when CS₂ was co-deposited with H atoms at higher flux, we expect that some reaction intermediates such as HC(S)SH and CH₂(SH)₂, which can form at an earlier stage of the reaction sequence (Figure 1), can remain intact in the reaction products. Indeed, new characteristic bands appeared on the ice substrate (Figure 6a), which were not observed at lower CS₂ deposition rates (see Figure 4).

After the co-deposition at the high CS₂/H ratio for 2 hours, new absorption peaks appeared in the 1270 - 1220 cm⁻¹ and 1100 - 1000 cm⁻¹ regions, which are likely to be attributed to sulfur-bearing products. Figure 6b displays the variation in the FTIR spectra with increasing the substrate temperature. As the surface temperature increases, new absorption features appear, likely due to the accumulation of products in the bulk CS₂ after its desorption. The assignment of the absorption peak at 1287 cm⁻¹, which gradually increased with temperature up to 180 K, might be attributed to the C-H rocking vibrational band of HC(S)SH (Lignell et al. 2021). The band at 1044 cm⁻¹ increased in intensity upon warming to 180 K (Figure 6b), supporting its assignment to the C=S stretching mode of HC(S)SH (Bohn et al. 1992; Lignell et al. 2021). According to our quantum chemical calculations, HC(S)SH can be formed through reaction (9).

Figure 6b also shows an absorption peak at 1029 cm⁻¹, which gradually appeared above 130 K during surface warm-up. In addition, a larger peak at 2522 cm⁻¹, emerging above 140 K, may also represent the S-H strength band of S-bearing products. Since H₂S and CH₃SH cannot remain on the substrate above 130 K, these absorption features are likely attributable to other S-H-bearing species. Moreover, the desorption temperatures of these bands were consistent with the desorption peak at *m/z* = 80 (see Figure 7), suggesting that they may be tentatively assigned to CH₂(SH)₂, which can be formed through reaction (11). Unfortunately, due to lack of reference data for the infrared feature of CH₂(SH)₂, the decisive identification of this molecules was not possible in the present study. Nevertheless, based on the computational and experimental results presented here, we strongly expect that CH₂(SH)₂, as well as HC(S)SH, is one of the possible candidates for the observed peaks even at high temperatures.

3.2.3 Comparison of the CS₂ depletion after exposure H and D atoms on c-ASW at 10 K

In Sections 3.1 and 3.2.1, we anticipate that, in order to activate CS₂, that is, to first hydrogenate the molecule and move *forward* in the reaction network, the system should overcome an activation energy of 13.1 kJ mol⁻¹ corresponding to reaction (8). To confirm such an expectation, we determined the kinetic isotopic effect (KIE) of the title reaction, that, as we see in Figure 1, is mostly dominated by the first hydrogenation. Figure 8 presents the change in the relative abundance of solid CS₂ after exposure to H and D atoms on c-ASW at 10 K. After up to 2 hours of exposure, the fractional loss of CS₂ was approximately 26% and 12% for exposure to H and D atoms, respectively. The loss of CS₂ is caused by the reaction with H (or D) atoms only; therefore, assuming that the reaction of CS₂ with H (or D) atoms proceeds through a single process where we merge all possible reactions, and the relative abundance of CS₂ can be represented by the following rate equation:

$$d[\text{CS}_2]/dt = -k_X[\text{X}][\text{CS}_2] \quad (19)$$

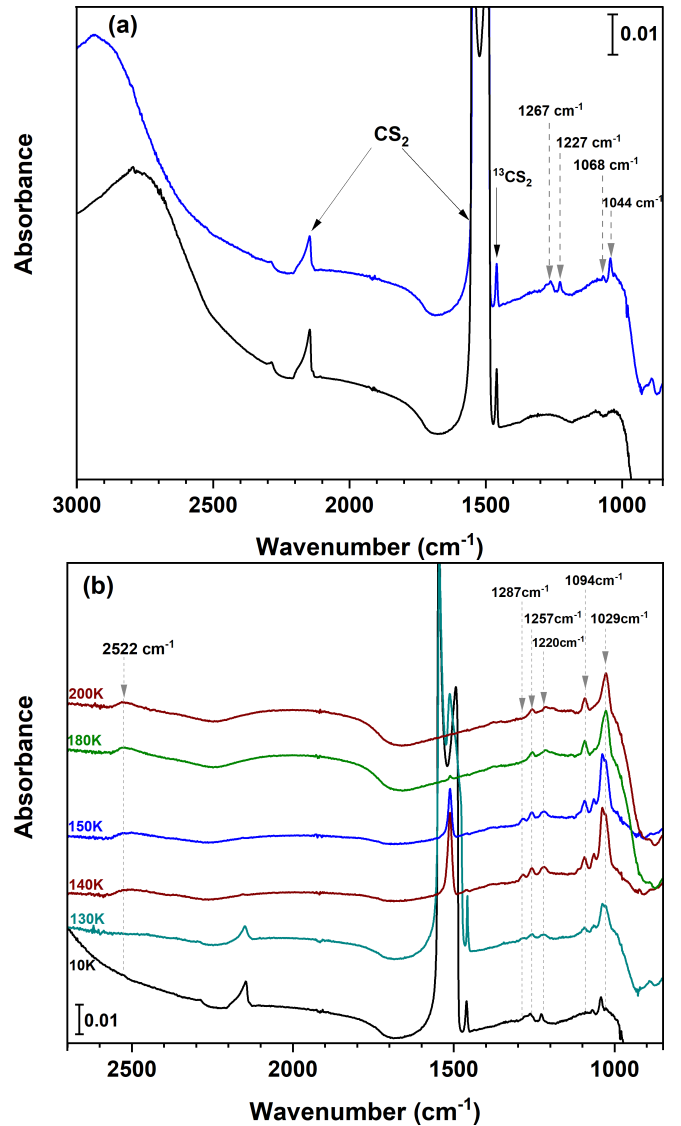


Figure 6. (a) FTIR spectrum of co-deposited CS₂ with H atoms (blue curve) after 2 hours under high deposition rate of 1 ML min⁻¹ compared with the co-deposition of CS₂ with H₂ (black curve) as a reference on c-ASW at 10 K. The dash arrows indicate the new features yielded through the reaction of CS₂ and H atoms. The solid arrows present remaining CS₂ on the substrate after 2 hours co-deposition with H/H₂. (b) Variation in the FTIR spectrum of products after the co-deposition of CS₂ with H atoms as the surface temperature was warmed up from 10 to 200 K.

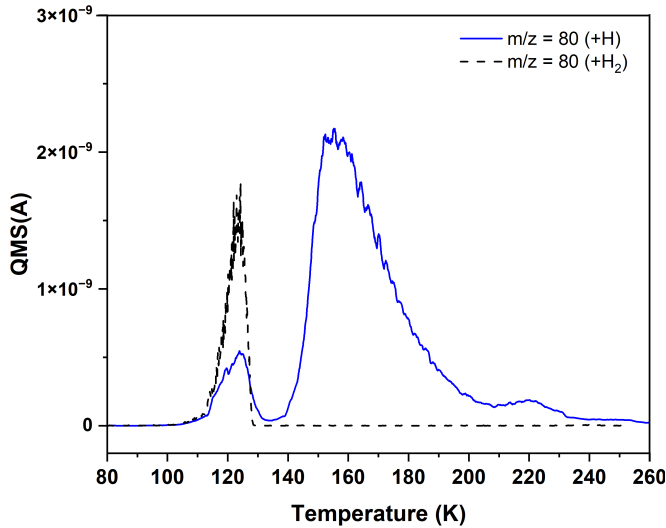
where [CS₂] and [X] are the surface number densities of CS₂ and X atoms (X = H or D) on the ice surface, respectively, and *k_X* is the rate coefficient for the X addition reactions. The reaction kinetics can be derived using the following integrated equations (20):

$$\Delta[\text{CS}_2]_t/[\text{CS}_2]_0 = A \times (1 - \exp(-k'_X t)), \quad (20)$$

where $\Delta[\text{CS}_2]_t$ is the change in the abundance of the solid CS₂ at time *t*, and [CS₂]₀ is the initial CS₂ abundance. *A* is the saturation value for the decrease in CS₂, and *k'_X* (= *k_X*[X]) is the effective rate constant for the reaction of CS₂ with X atoms. By fitting the data plot in Figure 8 using equation (20), we obtained the *k'_H* = (1.2 ± 0.1) × 10⁻³ s⁻¹ and *k'_D* = (2.0 ± 0.1) × 10⁻³ s⁻¹. According to the previous study

Table 2. Infrared Absorption band after co-deposition of CS₂ with H atoms on c-ASW

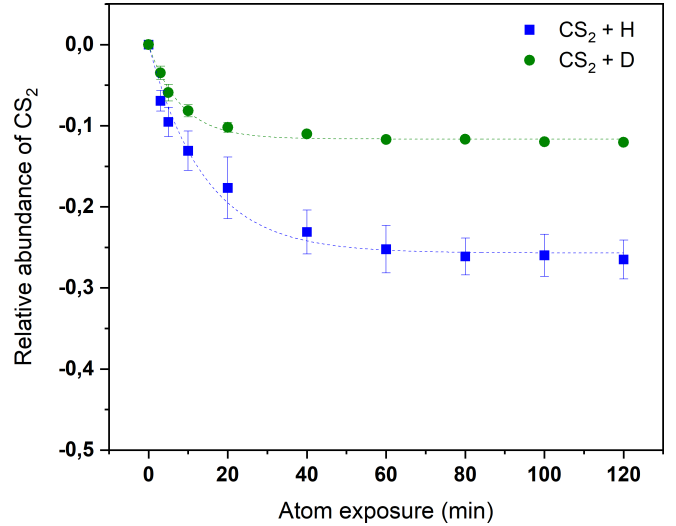
Band position (cm ⁻¹)	Assignment	References
1064 - 965	CH ₃ SH (CH ₃ - rocking)	Hudson (2016)
1044 - 1029	HC(S)SH (C-S str)	Bohn et al. (1992); Lignell et al. (2021)
1287	HC(S)SH (C-H)	Lignell et al. (2021)
1304	CH ₄ (C-H str)	Qasim et al. (2020); Nguyen et al. (2023)
1320	CH ₃ SH (-CH ₃ symm def)	Hudson (2016)
1442	CH ₃ SH (-CH ₃ bending)	Hudson (2016)
1540	CS ₂ (C=S str)	Garozzo et al. (2008); Edridge (2010)
2550	H ₂ S; CH ₃ SH (H-S str)	Fathe et al. (2006); Hudson (2016); Oba et al. (2019); Nguyen et al. (2023)
2838	H ₂ CS	Torres et al. (1982); Watanabe et al. (1991); Suzuki et al. (2007)
2914	unknown	
2929	CH ₃ SH (-CH ₃ symm str)	Hudson (2016); Nguyen et al. (2023)
2969	H ₂ CS (CH ₂ - symm str)	Torres et al. (1982); Watanabe et al. (1991); Suzuki et al. (2007)
2997	CH ₃ SH (-CH ₃ antisymm str)	Hudson (2016); Nguyen et al. (2023)

**Figure 7.** TPD-QMS profile of the desorption peak at $m/z = 80$ (for CH₂(SH)₂) after co-deposition of CS₂ with H atoms (solid blue line), compared with H₂ (dashed black line), at 10 K for up to 2 h.

of Kuwahata et al. (2015), when the flux of atoms was on the order to 10^{14} atoms cm⁻² s⁻¹, the number densities of H and D atoms ([D]/[H]) on porous amorphous solid water and crystalline water ices was ~ 4 and ~ 10 , respectively. By simply assuming that the [D]/[H] on c-ASW is the value between 4 and 10, for example 7, we estimate the ratio of k_D/k_H from the k'_D/k'_H , following the relationship:

$$\frac{k_D}{k_H} = \frac{k'_D}{k'_H} \times \frac{[H]}{[D]} = 1.7 \times \frac{1}{7} = 0.24 \quad (21)$$

Based on the assumption, the ratio of k_D/k_H obtains a value of 0.24, indicating that the D addition reaction of solid CS₂ is slower than the H addition reaction. This fraction, or more precisely its inverse (~ 4.2), represents the KIE, which, in the case of these reactions, is attributed to the influence of quantum tunneling. Although this KIE

**Figure 8.** Relative abundance of solid CS₂ on c-ASW with exposure to H (blue squares) and D (green circles) atoms at 10 K. The dash lines are the fits to Equation (20).

is relatively small, it is still noticeable, confirming that the reaction efficiency can be attributed to this effect. However, we note that it is derived from the overall decay of the [CS₂]_H/[CS₂]_D band, rather than from individual reaction pathways.

4 ASTROPHYSICAL IMPLICATIONS

The target molecule of this study, CS₂ has so far played a more significant role in cometary ices than in interstellar ices, as it has not been detected in interstellar environments. In fact, the astronomical detection of CS₂ in the gas phase is completed by the fact that it is a non-polar molecules, while detection in ices via IR vibrational bands has so far proven unsuccessful. Despite this hardships, models predict CS₂ can reach a total (gas + ice) fractional abundance of $\sim 10^{-10}$ (Laas & Caselli 2019). In fact, CS₂ is likely to be destroyed

through reactions with atoms such as oxygen and/or hydrogen on dust grains. In particular, reactions between CS₂ with O at thermal conditions can yield OCS on interstellar dust grains (Ward et al. 2012). In the case of reactions with atomic hydrogen, which are the purpose of this study, CS₂ can react through reactions (8) - (14), CS₂ will be consumed on dust grains, leading to the formation of other S-bearing species, including CH₃SH, H₂S, HC(S)SH, and CH₂(SH)₂ (see Table 1). If chemical routes of CS₂ proceed efficiently on dust grains, the production of S-bearing species would be controlled by the abundance of hydrogen atoms available to react with CS₂ molecules. Destruction reactions produce CS/H₂CS and H₂S, resulting in the cleavage of the original molecular skeleton. The CS/H₂CS molecules are then directly related with CS₂ and would be hydrogenated to yield CH₃SH (Lamberts 2018). Meanwhile, a fraction of H₂S will be released into the gas phase by chemical desorption (Oba et al. 2018). Previous studies (Nguyen et al. 2021; Molpeceres et al. 2021c; Nguyen et al. 2023, 2024) demonstrated that the hydrogenation of key S-bearing species, including OCS, CH₃SH, SO₂, and CS₂, lead to the formation of H₂S. The efficient conversion of sulfur species, including organosulfur compounds, to H₂S might be one of the, surely multicausal, explanations for the non-detection of S-bearing species in the solid state.

A possible way to provide some insights on CS₂ in the gas phase could be obtained from the observation of its protonated species, HSCS⁺. Unfortunately, this species has a very low dipole moment along the a-axis of 0.19D. Moreover, only transitions of a-type have been observed in the laboratory (McCarthy et al. 2009). Although, a larger dipole moment along the b-axis is expected, the frequencies of the b-type transitions remain unknown. From the a-type transitions, and using the ultrasensitive line survey QUIJOTE (Cernicharo et al. 2021d), we obtain a 3 sigma upper limit to the abundance of HSCS⁺ in the gas phase of $2 \times 10^{12} \text{ cm}^{-2}$ for each line in the survey. Averaging of the lines J=5-4 to J=8-7, the 3 sigma upper limit to the column density of CS₂ is $1 \times 10^{12} \text{ cm}^{-2}$. Protonated species have abundances between 50 and 100 times lower than the corresponding neutrals. Hence, the upper limit to CS₂ in the gas-phase is not very constraining in TMC-1, of the order of $50\text{-}100 \times 10^{12} \text{ cm}^{-2}$, which is a consequence of the low dipole moment of the protonated molecule.

The hydrogenation of CS₂ on interstellar dust grains leads to the formation of two molecules that can be considered more complex than the parent species: HC(S)SH and CH₂(SH)₂. It is therefore reasonable to explore whether these molecules may be present in the interstellar medium (ISM). Although current spectroscopic data are insufficient to enable the detection of CH₂(SH)₂, the presence of HC(S)SH has recently been reported by Manna & Pal (2024) in the hot core NGC 1333 IRAS 4A2. We have searched for HC(S)SH in TMC-1 using data from the QUIJOTE line survey (Cernicharo et al. 2022). These observations yielded no detection, as detailed in Appendix A. The non-detection of HC(S)SH can be attributed to several factors, but is nevertheless consistent with our findings, particularly the small energy barrier calculated for Reaction 10. This low barrier facilitates the rapid hydrogenation of HC(S)SH, leading to its efficient destruction. This interpretation is supported by our experimental results, where HC(S)SH is only observed in co-deposition experiments and only in small quantities. At higher temperatures, such as those characteristic of hot cores, the hydrogenation of HC(S)SH may proceed even in the gas phase, potentially yielding bimolecular products. This hypothesis warrants further investigation through laboratory experiments or accurate rate constant calculations. Similar considerations apply to CH₂(SH)₂. Although the reaction barrier for its hydrogenation is larger and its destruction in the gas phase may not be as efficient, hydrogenation on icy grain surfaces is expected to

proceed rapidly. This process likely forms SCH₂SH (see Reaction 12) and ultimately yields H₂S and H₂CS after a final hydrogenation step. These findings convey a twofold message. First, we demonstrate that hydrogenation of CS₂ efficiently destroys the S=C=S functional group. Second, the hydrogenation of not only CS₂ but also its reaction intermediates raises serious doubts about the long-term stability of the hydrogenation products HC(S)SH and CH₂(SH)₂ in the ISM. In particular, additional observational and modelling efforts are required to confirm the recent detection of HC(S)SH toward NGC 1333 IRAS 4A2 (Manna & Pal 2024).

5 CONCLUSION

The chemical pathways of CS₂ with H atoms in interstellar ices at low temperatures have been investigated. The hydrogenation of CS₂ leads to multiple reaction channels, including the formation of H₂S and CH₃SH, as well as HC(S)SH and CH₂(SH)₂. According to quantum chemical calculations, these species can form on dust grain surfaces via low-barrier or barrierless reactions, with their formation efficiencies dependent on the local abundance of CS₂. The non-detection of CS₂ in interstellar ices can therefore be attributed to its efficient destruction. In regards the formation of HC(S)SH and CH₂(SH)₂ compounds from CS₂ under ISM conditions, the extrapolation of our experimental and theoretical results suggest that these molecules should not withstand a wide array of standard chemical conditions in the ISM, including cold and hot cores.

ACKNOWLEDGEMENTS

This work was partly supported by JSPS KAKENHI grant Nos. JP25H00677, JP23H03980, JP21H04501 (to Y.O.), JP22H00159 (to N.W.), and JP21F21319 (to T.N., N.W.). GM acknowledges the support of the grant RYC2022-035442-I funded by MICIU/AEI/10.13039/501100011033 and ESF+. GM also received support from project 20245AT016 (Proyectos Intramurales CSIC). We acknowledge the computational resources provided the DRAGO computer cluster managed by SGAI-CSIC, and the Galician Supercomputing Center (CESGA). The supercomputer FinisTerra III and its permanent data storage system have been funded by the Spanish Ministry of Science and Innovation, the Galician Government, and the European Regional Development Fund (ERDF). MA and JC thank Spanish Ministerio de Ciencia, Innovación, y Universidades for funding through the project PID2023-147545NB-I00. GE acknowledges support from Spanish grant PID2022-137980NB-I00, funded by MCIN/AEI/10.13039/501100011033/FEDER UE. We also thank ERC for funding through grant ERC-2013-Syg-610256-NANOCOSMOS. The observations of TMC-1 molecular cloud are carried out with the Yebes 40m telescope (projects 19A003, 20A014, 20D023, 21A011, 21D005, and 23A024). The 40m radio telescope at Yebes Observatory is operated by the Spanish Geographic Institute (IGN; Ministerio de Transportes, Movilidad y Agenda Urbana).

DATA AVAILABILITY

The underlying data supporting the results of this article will be shared on request.

References

- Agúndez M., Marcelino N., Tercero B., Jiménez-Serra I., Cernicharo J., 2023, *A&A*, **677**, A106
- Agúndez M., Molpeceres G., Cabezas C., Marcelino N., Tercero B., Fuentetaja R., de Vicente P., Cernicharo J., 2025, *A&A*, **693**, L20
- Anderson D. E., Bergin E. A., Maret S., Wakelam V., 2013, *ApJ*, **779**, 141
- Bak B., Nielsen O. J., Svanholt H., 1978, *J. Mol. Spectrosc.*, **69**, 401
- Basalgète R., Free V., Poirat L., Krim L., 2026, *A&A*
- Bockelée-Morvan D., et al., 2000, *A&A*, **353**, 1101
- Bohn R. B., Brabson G. D., Andrews L., 1992, *J. Phys. Chem.*, **96**, 1582
- Cabezas C., Agúndez M., Endo Y., Tercero B., Lee Y.-P., Marcelino N., de Vicente P., Cernicharo J., 2024, *A&A*, **686**, L3
- Cabezas C., et al., 2025, *A&A*, **698**, L24
- Cataldo F., 1995, *Inorg. Chim. Acta*, **232**, 27
- Cernicharo J., et al., 2021a, *A&A*, **648**, L3
- Cernicharo J., et al., 2021b, *A&A*, **648**, L3
- Cernicharo J., Cabezas C., Endo Y., Agúndez M., Tercero B., Pardo J. R., Marcelino N., de Vicente P., 2021c, *A&A*, **650**, L14
- Cernicharo J., Agúndez M., Kaiser R. I., Cabezas C., Tercero B., Marcelino N., Pardo J. R., de Vicente P., 2021d, *A&A*, **652**, L9
- Cernicharo J., Agúndez M., Kaiser R. I., Cabezas C., Tercero B., Marcelino N., Pardo J. R., de Vicente P., 2021e, *A&A*, **652**, L9
- Cernicharo J., Agúndez M., Cabezas C., Marcelino N., Tercero B., Pardo J. R., Fuentetaja R., de Vicente P., 2022, *EPJ Web of Conferences*, **265**, 00041
- Cernicharo J., Agúndez M., Cabezas C., Tercero B., Fuentetaja R., Marcelino N., de Vicente P., 2024a, *A&A*, **682**, L4
- Cernicharo J., Cabezas C., Agúndez M., Fuentetaja R., Tercero B., Marcelino N., de Vicente P., 2024b, *A&A*, **688**, L13
- Cernicharo J., Cabezas C., Agúndez M., Fuentetaja R., Tercero B., Marcelino N., de Vicente P., 2024c, *A&A*, **688**, L13
- Despois D., Crovisier J., Bockelée-Morvan D., Colom P., 1992, in *Symposium-International Astronomical Union*. pp 459–460
- Edridge J. L., 2010, PhD thesis, UCL (University College London)
- Esplugues G., Agúndez M., Molpeceres G., Tercero B., Cabezas C., Marcelino N., Fuentetaja R., Cernicharo J., 2025, *A&A*, **699**, L2
- Fathe K., Holt J. S., Oxley S. P., Pursell C. J., 2006, *J. Phys. Chem. A*, **110**, 10793
- Feldman P. D., et al., 1980, *Nat*, **286**, 132
- Felix L., Kitzmann D., Demory B.-O., Mordasini C., 2025, Evidence for sulfur chemistry in the atmosphere of the warm sub-Neptune TOI-270 d ([arXiv:2504.13039](https://arxiv.org/abs/2504.13039))
- Ferrante R. F., Moore M. H., Spiliotis M. M., Hudson R. L., 2008, *ApJ*, **684**, 1210
- Fuente A., et al., 2023, *A&A*, **670**, A114
- Furuya K., Oba Y., Shimonishi T., 2022, *ApJ*, **926**, 171
- Garozzo, M. Fulvio, D. Kanuchova, Z. Palumbo, M. E. Strazzulla, G. 2010, *A&A*, **509**, A67
- Garozzo M., Fulvio D., Gomis O., Palumbo M. E., Strazzulla G., 2008, *Planet. Space Sci.*, **56**, 1300
- Gerakines P. A., Schutte W. A., Greenberg J. M., van Dishoeck E. F., 1995, *A&A*, **296**, 810
- Herath A., et al., 2025, *Nat. Commun.*, **16**, 5571
- Heymann D., Cataldo F., Thiemens M. h., Fokkens R., Nibbering N. m. m., Vis R. d., 2000, *Meteorit. Planet. Sci.*, **35**, 355
- Hudson R., 2016, *Physical Chemistry Chemical Physics*, **18**, 25756
- Jiménez-Escobar A., Muñoz Caro G. M., Chen Y. J., 2014, *MNRAS*, **443**, 343
- Kuwahata K., Hama T., Kouchi A., Watanabe N., 2015, *Phys. Rev. Lett.*, **115**, 133201
- Laas J. C., Caselli P., 2019, *A&A*, **624**, A108
- Lamberts T., 2018, *A&A*, **615**, L2
- Lamberts T., Kästner J., 2017, *J. Phys. Chem. A*, **121**, 9736
- Lignell A., Osadchuk I., Räsänen M., Lundell J., 2021, *ApJ*, **917**, 68
- Maeda S., Ohno K., Morokuma K., 2013, *Phys. Chem. Chem. Phys.*, **15**, 3683
- Maeda S., Harabuchi Y., Sumiya Y., et al., 2023a, *GRRM23*
- Maeda S., Harabuchi Y., Hayashi H., Mita T., 2023b, *Annu. Rev. Phys. Chem.*, **74**, 287
- Manna A., Pal S., 2024, *ACS Earth Space Chem*, **8**, 2401
- Mardirossian N., Head-Gordon M., 2016, *J. Chem. Phys.*, **144**, 214110
- Martín-Doménech R., Öberg K. I., Muñoz Caro G. M., Carrascosa H., Fuente A., Rajappan M., 2024, *MNRAS*, **535**, 807
- McCarthy M. C., Thaddeus P., Wilke J. J., Schaefer Henry F. I., 2009, *The Journal of Chemical Physics*, **130**, 234304
- Mifsud D. V., et al., 2021, *Space Sci. Rev.*, **217**, 14
- Mifsud D. V., et al., 2022, *Frontiers in Chemistry*, Volume 10 - 2022
- Mifsud D. V., et al., 2024, *Icarus*, **411**, 115926
- Mifsud D. V., et al., 2025, *ACS Earth Space Chem.*, **9**, 1227
- Millar T. J., Herbst E., 1990, *A&A*, **231**, 466
- Millar T. J., Adams N. G., Smith D., Lindinger W., Villinger H., 1986, *MNRAS*, **221**, 673
- Molpeceres G., Kästner J., Fedoseev G., Qasim D., Schömig R., Linnartz H., Lamberts T., 2021a, *J. Phys. Chem. Lett.*, **12**, 10854
- Molpeceres G., de la Concepción J. G., Jiménez-Serra I., 2021b, *ApJ*, **923**, 159
- Molpeceres G., García de la Concepción J., Jiménez-Serra I., 2021c, *ApJ*, **923**, 159
- Molpeceres G., et al., 2022, *A&A*, **663**
- Molpeceres G., Tsuge M., Furuya K., Watanabe N., San Andrés D., Rivilla V. M., Colzi L., Aikawa Y., 2024, *J. Phys. Chem. A*, p. acs.jpca.3c08286
- Molpeceres G., Enrique-Romero J., Ishibashi A., Oba Y., Hidaka H., Lamberts T., Aikawa Y., Watanabe N., 2025, *MNRAS*, **538**, 1565
- Moses J., et al., 2024, in *AAS/Division for Planetary Sciences Meeting Abstracts*. p. 308.06
- Nagaoka A., Watanabe N., Kouchi A., 2007, *JPCA*, **111**, 3016
- Neese F., 2022, *WIREs Comput. Mol. Sci.*, **12**, e1606
- Nguyen T., Oba Y., Shimonishi T., Kouchi A., Watanabe N., 2020, *ApJ*, **898**, L52
- Nguyen T., Oba Y., Sameera W. M. C., Kouchi A., Watanabe N., 2021, *ApJ*, **922**, 146
- Nguyen T., Oba Y., Sameera W. M. C., Furuya K., Kouchi A., Watanabe N., 2023, *ApJ*, **944**, 219
- Nguyen T., Oba Y., Sameera W. M. C., Furuya K., Watanabe N., 2024, *ApJ*, **976**, 250
- Oba Y., Miyauchi N., Hidaka H., Chigai T., Watanabe N., Kouchi A., 2009, *ApJ*, **701**, 464
- Oba Y., Osaka K., Watanabe N., Chigai T., Kouchi A., 2014, *FaDi*, **168**, 185
- Oba Y., Tomaru T., Lamberts T., Kouchi A., Watanabe N., 2018, *Nat. Astron.*, **2**, 228
- Oba Y., Tomaru T., Kouchi A., Watanabe N., 2019, *ApJ*, **874**, 124
- Öberg K. I., Garrod R. T., van Dishoeck E. F., Linnartz H., 2009, *A&A*, **504**, 891
- Prudeniano D., et al., 2018, *A&A*, **612**, A56
- Qasim D., Fedoseev G., Chuang K. J., He J., Ioppolo S., van Dishoeck E. F., Linnartz H., 2020, *Nat. Astron.*, **4**, 781
- Rappoport D., Furche F., 2010, *J. Chem. Phys.*, **133**, 134105
- Ruffle D. P., Hartquist T. W., Caselli P., Williams D. A., 1999, *MNRAS*, **306**, 691
- Shingledecker C. N., Lamberts T., Laas J. C., Vasyunin A., Herbst E., Kästner J., Caselli P., 2020, *ApJ*, **888**, 52
- Slavicska K., et al., 2025, *A&A*, **693**, A146
- Smith A. M., Stecher T. P., Casswell L., 1980, *ApJ*, **242**, 402
- Suzuki E., Yamazaki M., Shimizu K., 2007, *Vibrational spectroscopy*, **43**, 269
- Torres M., Safarik I., Clement A., Strausz O., 1982, *Can. J. Chem.*, **60**, 1187
- Tsuge M., Lee Y.-P., 2017, *Phys. Chem. Chem. Phys.*, **19**, 9641
- Tsuge M., Molpeceres G., Aikawa Y., Watanabe N., 2023, *Nat. Astron.*
- Vidal T. H. G., Loison J.-C., Jaziri A. Y., Ruaud M., Gratier P., Wakelam V., 2017, *MNRAS*, **469**, 435
- Wakelam V., Castets A., Ceccarelli C., Lefloch B., Caux E., Pagani L., 2004, *A&A*, **413**, 609
- Ward M. D., Hogg I. A., Price S. D., 2012, *MNRAS*, **425**, 1264
- Watanabe O., Suzuki E., Watari F., 1991, *Bull. Chem. Soc. Jpn.*, **64**, 1389
- Watanabe N., Nagaoka A., Hidaka H., Shiraki T., Chigai T., Kouchi A., 2006, *P&SS*, **54**, 1107

Weaver H., Feldman P., Festou M., A'Hearn M., Keller H., 1981, *Icarus*, 47, 449

APPENDIX A: SEARCH FOR HCSSH IN TMC-1

We have searched for the trans isomer of dithioformic acid, which is the most stable form, in the cold starless core TMC-1, where a large variety of sulfur-containing molecules have been found (Cernicharo et al. 2021b, 2024c; Agúndez et al. 2025; Cabezas et al. 2025; Esplugues et al. 2025). The rotational spectrum of trans HCSSH has been measured in the laboratory (Prudenzano et al. 2018) and the dipole moment components along the a and b axes are 1.53 D, as measured by Bak et al. (1978), and 0.1924 D, as calculated by Prudenzano et al. (2018). The most favorable lines of trans HCSSH in the Q band (31.0-50.3 GHz) are a -type transitions with $K_a = 0, 1$. We have searched for them without success in our QUIJOTE data of TMC-1 observed with the Yebes 40m telescope (Cernicharo et al. 2021e). Assuming a rotational temperature of 9 K, equal to the gas kinetic temperature in TMC-1, an emission size with a diameter of 80'', and a line width of 0.60 km s⁻¹ (Agúndez et al. 2023), we derive a 3σ upper limit to the column density of trans HCSSH of 3.5×10^{10} cm⁻². Therefore, we could not detect thioformic acid in TMC-1. The HCSSH/HCOOH abundance ratio in TMC-1 is $< 2.5 \times 10^{-2}$, similar to the CH₃SH/CH₃OH and CH₃CHS/CH₃CHO ratios found in this same source (Agúndez et al. 2025).

This paper has been typeset from a TeX/L^AT_EX file prepared by the author.

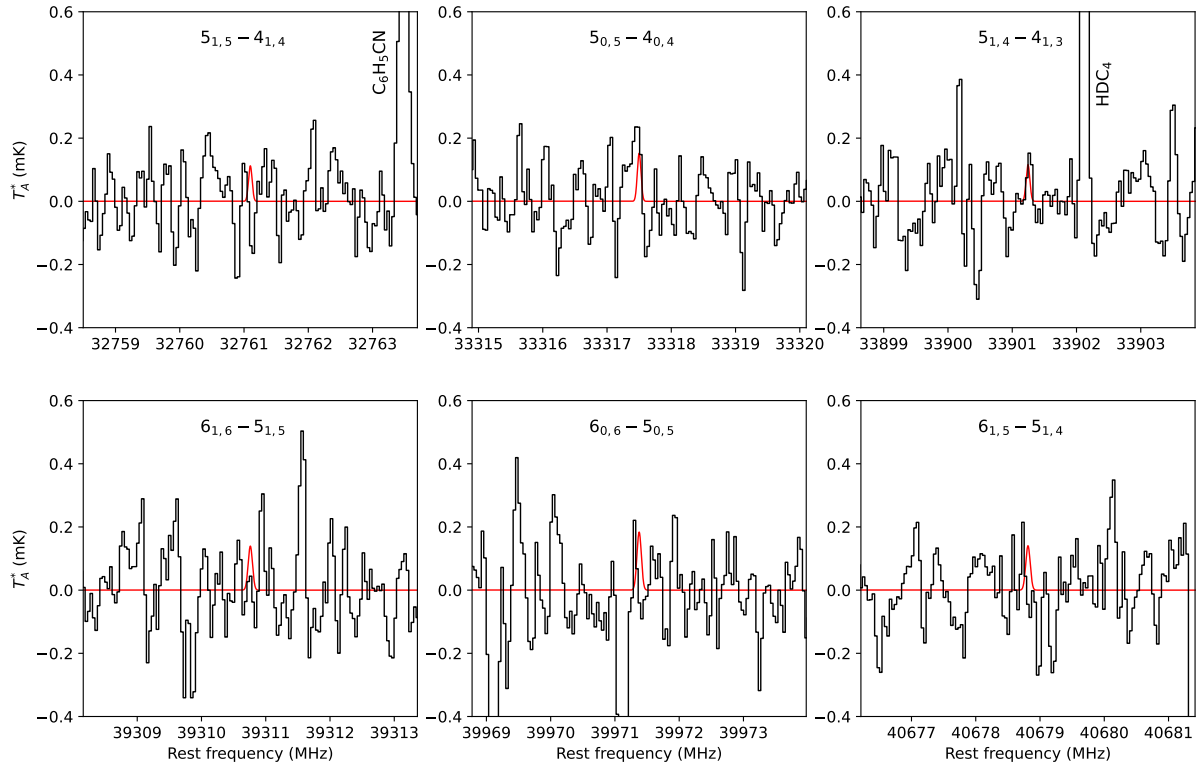


Figure A1. Spectra taken with the Yebes 40m telescope toward TMC-1 at the frequencies of the more favorable lines of trans HC(S)SH. We also show in red the calculated spectrum under thermodynamic equilibrium, adopting as column density the 3σ upper limit given in the text.